Research

Thermally induced Fe_2O_3 spikes decorated Ag/Fe_2O_3 nanocomposite fabrication for anti-bacterial and anti-cancer activities

Md. Kaium Hossain[1,2] · Anshuman Mishra[3] · Aanshi Tiwari[3] · Bishweshwar Pant[4] · Shaikat Chandra Dey[2,5] · Ayushi Tiwari[3] · Otun Saha[7] · Md. Mizanur Rahaman[6] · Yogesh R. Shukla[3] · Ashutosh Tiwari[3] · Md. Ashaduzzaman[2,3,8]

Received: 8 September 2023 / Accepted: 13 November 2023
Published online: 16 November 2023

Abstract
In the context of anti-cellular catalytic permutations, the development of thermally-induced nanotechnology is of great importance. In this study, iron oxides (Fe_2O_3) decorated silver (Ag) core–shell nanocomposite was prepared using a green thermal decomposition process without using any additional chemicals. The nanocomposite was characterized for its composition, phase interactions, morphology, and stability using spectroscopic, thermogravimetric, and microscopic techniques. The resultant nanocomposite were also investigated against different types of bacteria and cancer cell lines. Both Gram-positive bacteria (*Staphylococcus aureus*) and Gram-negative bacteria (*Klebsiella spp., E. coli*, and *Pseudomonas*) growth was inhibited by the Ag/Fe_2O_3 nanocomposite. The highest 19 mm zone of inhibition (ZOI) was found for *Staphylococcus aureus* by the combined effect of Ag and Fe_2O_3. The antibiofilm efficacy of the prepared nanocomposites showed biofilm destruction of 82.56% *Staphylococcus aureus* and 51.06% *Klebsiella spp.* Furthermore, the nanocomposite resulted in 80–90% death of Hela and BHK-21 cells but displayed lower cell toxicity in the case of the Vero cell line. This pathway of nanocomposites preparation with particle surface engineering would open new doors in the fields of nanobiotechnology and nanobiomedical applications.

Keywords Ag/Fe_2O_3 nanocomposite · Thermally induced nanocomposite · Anti-bacterial · Antibiofilm · Cytotoxicity

1 Introduction

Composite nanomaterial containing metal and magnetic nanocrystals has attracted much interest because they offer multifunctional applications. In the early 1990s, researchers further targeted to improve the function of these nanomaterials by preparing multilayered nanocomposites [1]. Fe_2O_3 nanoparticle possesses both magnetic and semiconductor properties, which lead to multifunctional biomedical applications such as anti-bacterial, anti-fungal, anti-cancer activity, targeted drug delivery, etc. In addition to that, Fe_2O_3 nanoparticles are nontoxic in nature and environment friendly [2]. Silver is reported as one of the most promising metal nanoparticle

Supplementary Information The online version contains supplementary material available at https://doi.org/10.1007/s42452-023-05599-y.

✉ Ashutosh Tiwari, director@iaam.se; ✉ Md. Ashaduzzaman, azaman01@du.ac.bd | [1]Department of Chemistry, Bangladesh University of Engineering and Technology, Dhaka 1000, Bangladesh. [2]Department of Applied Chemistry and Chemical Engineering, University of Dhaka, Dhaka 1000, Bangladesh. [3]Institute of Advanced Materials, IAAM, Gammalkilsvägen 18, 590 53 Ulrika, Sweden. [4]Woosuk University, Wanju 55338, Republic of Korea. [5]Department of Forest Biomaterials, North Carolina State University, Campus Box 8005, Raleigh, NC 27695, USA. [6]Department of Microbiology, University of Dhaka, Dhaka 1000, Bangladesh. [7]Department of Microbiology, Noakhali Science and Technology University, Noakhali 3814, Bangladesh. [8]Comilla University, Cumilla 3506, Bangladesh.

due to its high anti-microbial and cytotoxic properties from the ancient time. So, the combined effect of Ag and Fe_2O_3 are gaining the attention of researchers because of their unique catalytic activity, anti-bacterial activity, and bio-imaging ability [3].

To date, several different synthetic methods including co-precipitation, ultrasonic cavitation, hydrothermal synthesis, and microwave-assisted synthesis, have been developed for the purpose of fabricating silver nanoparticles (Ag NPs) decorated with iron oxide composites (Ag/Fe_2O_3). For example, Saranya et al. [4] synthesized Fe_2O_3/Ag nanocomposites in a 2:1 ratio of iron oxide, silver precursors using one pot microwave-assisted green synthesis method and Khan et al. [5] used co-reduction method to prepare Fe_2O_3/Ag nanocomposite with *Algaia Monozyga* leaves extract. For the preparation of hematite-silver heterodimer, Trang et al. [6] employed a simple two-step hydrothermal synthesis approach. Recently, Al-Zahrani et al. [7] phytosynthesized Ag/Fe_2O_3 nanocomposite using the extract of *Buddleja lindleyana*. They applied these nanocomposites for anti-cancer and anti-microbial applications. Although Fe_2O_3 performance was highly improved by adding Ag NP in several studies, nanocomposite fabrication is usually a multi-step process. Therefore, it is important to engineer the Ag/Fe_2O_3 nanocomposite with an easy and environmentally friendly method.

In this paper, we have synthesized Fe_2O_3 nanospike-loaded Ag NP following a facile thermal decomposition method. This method did not require the use of a reducing agent or any other additional chemicals. Compared to other conventional synthesis methods, thermal decomposition is relatively simple, cost-effective, environmentally friendly, and the purity of the product is high [8]. In the preparation of this nanocomposite, the ratio of precursor materials (Fe_2O_3 and $AgNO_3$) was adjusted to 2:1 and 1:1 to see the difference in size, structure, morphology, and the effectiveness of these composites in various applications. After the nanocomposite was formed, the free Fe_2O_3 was removed and a nanospike-like surface was formed by treating it with conc. HCl. A sustainable green approach to synthesize and apply in biological activities (such as anti-bacterial, anti-cancer, etc.) are important aspects that can contribute in a more ecological way to provide sustainable healthcare management in the form of diagnosis devices as a significant aspect [9, 10]. The nanocomposite that was produced was tested for its effectiveness in controlling the growth of both Gram-positive (*Staphylococcus aureus*) and Gram-negative (*Klebsiella spp.*, *E. coli*, *Pseudomonas*) bacteria, including their biofilms through its anti-microbial and anti-biofilm properties and the efficacy of different types of produced nanocomposite was also compared. It was observed that the composite showed greater activity towards bacteria than the individual materials, and with increasing the concentration, the activity increases. In addition to anti-bacterial and anti-biofilm activity, cytotoxicity of the produced nanocomposite was also investigated against Vero, Hela, and BHK-21 cell lines to determine its activity towards cancer cell and biocompatibility. The composite showed significant toxicity towards Hela and BHK-21 but shows lower toxicity against the Vero cell line. Furthermore, plausible mechanisms for anti-microbial activity have been proposed.

2 Experimental

2.1 Materials

Ferric oxide red (extra pure, 95%), silver nitrate (extra pure, 99%) were purchased from LOBA Chemie Pvt. Ltd, India. Hydrochloric acid (37%) was acquired from Merck KGaA (64271 Darmstadt, Germany). Mueller–Hinton agar and Tryptic Soy Agar (TSA) were used from Oxoid Limited, UK, and Sigma Aldrich, respectively. The microbial samples were taken from the Department of Microbiology, University of Dhaka, Bangladesh. All Chemicals used in the study were of analytical grade and used without further purification. Deionized water was used in all experiments.

2.2 Synthesis of Ag/Fe_2O_3 nanocomposite

The Ag/Fe_2O_3 nanocomposite was synthesized directly by the thermal decomposition method, where Fe_2O_3 was well mixed and ground with a calculated amount of $AgNO_3$ to produce a weight ratio of 2:1 and 1:1 of Fe_2O_3 and Ag in the product. Two crucibles were used to prepare the samples, which were then separately heated in a muffle furnace for 1 h at 500 °C. After the furnace was cooled to room temperature, they were treated with conc. HCl and was continuously stirred to remove free oxides present in the products. The product was washed several times with deionized water before drying at 105 °C. After drying, the product was ground to separate the agglomerated particles. Hereafter, products containing 2:1 and 1:1 ratios of Fe_2O_3 and Ag were named $IO_{82}S$ and $IO_{65}S$, respectively.

2.3 Characterization

To obtain the infrared spectra of the nanocomposites, a Shimadzu IRPrestige21 spectrophotometer (Shimadzu Corporation, Japan) was used with measurements taken in the wavenumber range of 4000–400 cm^{-1}. Using an X-ray diffractometer (model U1tima IV, manufactured by Rigaku Corporation, Japan), the crystallinity of the products was measured within the temperature range of 20–70 °C. The X-ray diffraction (XRD) patterns of the nanocomposites

were obtained by scanning continuously within a range of 5 to 100°, with a scanning speed of 3% per minute. A thermogravimetric analyzer (TGA-50 Shimadzu, Japan) was utilized to measure the thermal breakdown behavior of the samples, with readings taken from 20 to 800 °C. The samples were subjected to a heating rate of 10 °C/min within an environment of nitrogen, using an alumina cell. Additionally, FE-SEM and EDS analyses of the sample were conducted using the JSM-7900F Schottky Field Emission Scanning Electron Microscope.

2.4 In vitro biological studies

2.4.1 Antibacterial effect evaluation

The Ag/Fe_2O_3 nanocomposite's ability to combat pathogenic bacteria was evaluated against Gram-negative bacteria strains *Klebsiella spp.* strain KH15, *E. coli* Strain EH9 and *Pseudomonas* spp. strain PsI1, which were previously identified as multidrug-resistant clinical isolates, as well as Gram-positive *Staphylococcus aureus* strain 6 s, frequently used for clinical sample analysis. These isolates were obtained from the Department of Microbiology at the University of Dhaka, Bangladesh. Five isolates were subjected to antibacterial sensitivity tests using the agar well diffusion method described by Bauer A, 1966 [11]. The three concentrations of Ag/Fe_2O_3 nanocomposites: 5, 20, and 30 mg/mL with and without controls were used in this study. The test materials were dispersed in distilled water and subjected to sonication for 30 min. Optical density (OD) 0.1 was adjusted on a UV–visible spectrophotometer (Spectrumlab 1200RS, Japan) for all bacterial cultures. *Escherichia coli* DH5α was used as a reference strain. The 100 µL of bacteria was consistently spread on Mueller–Hinton agar (MHA) plates from the respective bacterial culture, and a sterile cotton swab was used to coat the agar plate. In each agar plate, a sterile well cutter (7.0 mm diameter) was employed to create an aperture into which a suspension of nanoparticles was added for each bacterial strain. Optimal bacterial growth was achieved by incubation at 37 °C overnight, after which the clear zones around the well were assessed to determine the anti-bacterial activity of the Ag/Fe_2O_3 nanocomposites [12].

2.4.2 Anti-biofilm effect evaluation

The anti-biofilm activity of the Ag/Fe_2O_3 nanocomposites was evaluated by using a 96-well microtiter plate following the study by Mohanta et al. [13]. Kostaki et al.'s recommended method was employed to induce the formation of biofilm on the glass slides [14]. Once the biofilm was established, the glass slides were cleaned using a 70% alcohol solution, followed by exposure to UV radiation for a duration of 15 min. After growing on Tryptic Soy Agar (TSA) overnight at 37 °C, Gram-negative strains *E. coli* EH19, *Pseudomonas Spp*., and *Klebsiella* spp. KH15, as well as the Gram-positive strain *Staphylococcus aureus*, were stored at a temperature of 4 °C. After a total of 24 h, the isolated colonies were resuspended in 5 mL of tryptic soy broth (TSB) in order to produce an overnight culture that would result in the formation of biofilm. On glass coverslips, the treatment of biofilm with Ag/Fe_2O_3 nanocomposites was carried out. The coverslips were then placed in a 50 mL falcon tube, 15 mL of anti-bacterial agents were added, and the tube was centrifuged at 300 rpm for 5 min on a thermo centrifuge machine. This process was repeated three times after each washing with sterile water. Loosely attached cells were removed by washing with sterile water after taking these slips from falcon tubes. To count viable cells, agar plating was employed after a ten-fold dilution and subsequent incubation at 37 °C for 24 h. The number of colonies for each bacterial strain was expressed as colony-forming units per milliliter (CFU/mL). The nanocomposite's anti-biofilm activity was evaluated by calculating the survival fractions (SF) based on the ratio of untreated viable cells to treated viable cells, expressed as a percentage. The percentage killed (PK) was then calculated as $(1-SF)\times 100$ percent. The anti-biofilm efficacy of the nanocomposite was assessed using both the aforementioned method and the log reduction (LR) factor, which was determined using the formula $LR = Log10\ (1/SF)$, as previously described by Hamilton et al. [15].

2.4.3 Cytotoxic effect

The Vero (obtained from African green monkey kidney epithelial cells), Hela (human cervical carcinoma cells), and BHK-21 (derived from baby hamster kidney fibroblast cells) cell lines were grown in DMEM (Dulbecco's Modified Eagles' medium) supplemented with 1% penicillin–streptomycin (1:1), 0.2% gentamycin, and 10% FBS (fetal bovine serum). The cells were seeded into a 96-well plate at a density of Vero cells (1.5×104/100 µl), Hela cells (2.0×104/100 µL), and BHK-21 cells (1.5×104/100 µL), followed by incubation at 37 °C with 5% CO_2. On a subsequent day, an autoclaved sample of 25 µL was added to each well. Following 48 h of incubation, any insoluble samples were washed using fresh media, and an inverted light microscope was employed to assess sample cytotoxicity. For each sample, duplicate wells were employed.

3 Results and discussion

3.1 Structural characterization

3.1.1 Attenuated total reflection infrared (ATR-IR) spectroscopy

Figure 1a, b shows the ATR-IR spectra of Fe_2O_3 and prepared Ag/Fe_2O_3 nanocomposites. The spectra of Fe_2O_3 and both $IO_{82}S$ and $IO_{65}S$ showed absorption bands at 3358 cm^{-1}, which could be attributed to –OH stretching vibrations [16]. In the ATR-IR spectrum of Fe_2O_3 in its pure form, a prominent peak was observed at 549 cm^{-1}, indicating the stretching vibration of the Fe–O bond present in both tetrahedral and octahedral sites. Another peak was observed at 464 cm^{-1}, which corresponds to the bending vibration of the Fe–O bond [17, 18]. The spectral change from 549 to 590 cm^{-1} and from 464 to 482 cm^{-1} might be observed due to the incorporation of more silver since metal, which interacts with the vibration of Fe–O bond and causes a gradual spectral shift [3, 19]. These band changes and decreases in peak intensity for Fe–O vibration from Fe_2O_3 to $IO_{82}S$ and $IO_{65}S$ indicate successful incorporation of Ag with Fe_2O_3.

3.1.2 X-ray diffraction (XRD)

The XRD patterns of the simulated metallic Ag, commercial Fe_2O_3 and synthesized Ag/Fe_2O_3 nanocomposites are shown in Fig. 1c. All samples showed strong diffraction peaks, indicating good crystallinity. Similar peaks were observed for the $IO_{82}S$ and $IO_{65}S$ samples. In both samples, the peak appearing at the 2θ values of 24.2, 33.2, 57.5, and 64.2° is attributed to the (012), (104), (018), and (300) crystalline structures of Fe_2O_3, respectively. Besides these peaks, the crystallographic planes of Ag were detected at 2θ angles of 37.8, 44, and 64° representing (111), (200),

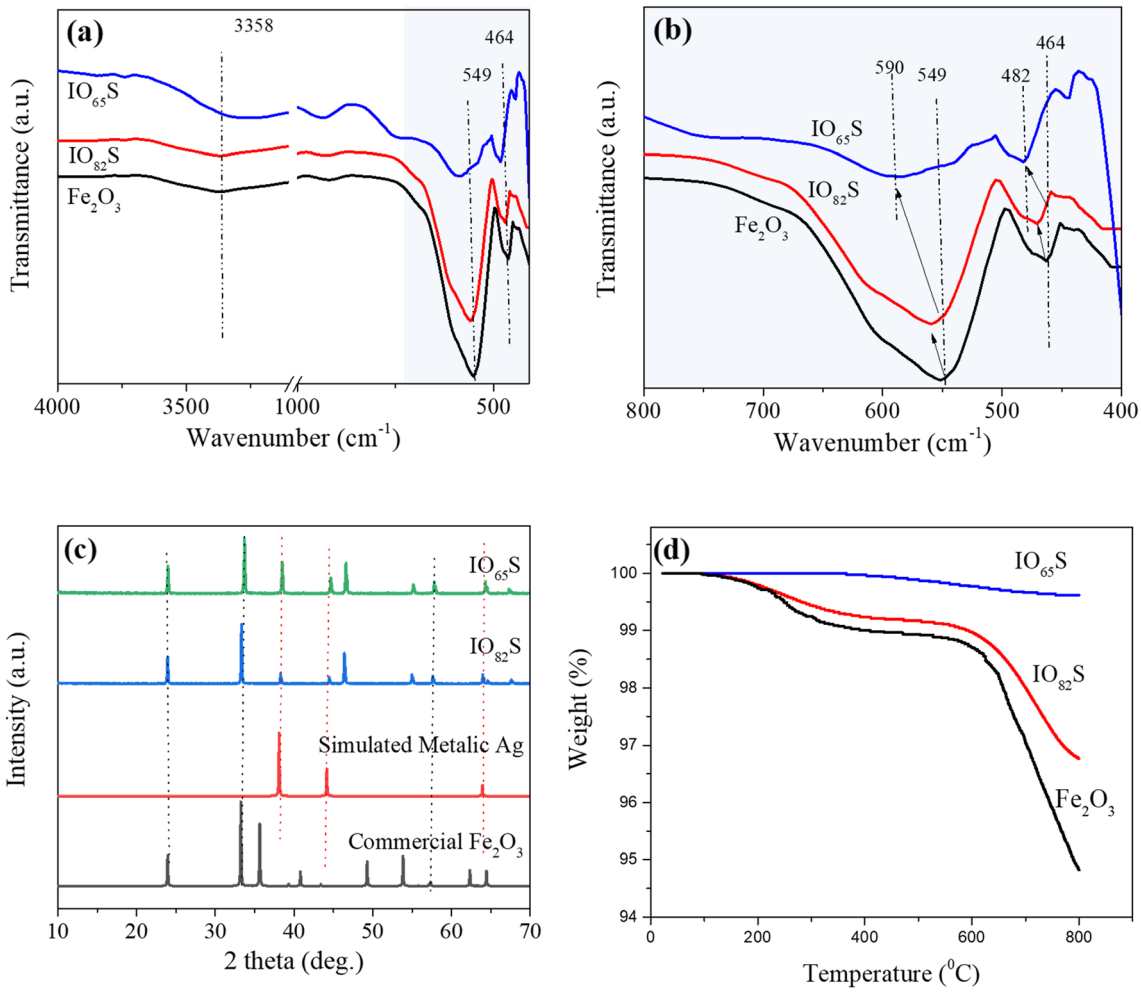

Fig. 1 **a**, **b** ATR-IR spectrum; **c** XRD diffraction pattern; **d** TGA thermogram of Fe_2O_3 and Ag/Fe_2O_3 nanocomposites

and (220) planes, respectively. By employing the Debye-Sherrer equation, the average crytallite size of the Fe_2O_3 nanospikes was estimated and was found to be approximately 82 nm for $IO_{82}S$ and around 65 nm for $IO_{65}S$ [20]. The high concentration of Ag in $IO_{65}S$ might prevent Fe_2O_3 nanospike agglomeration, thus reducing the crystal size of Fe_2O_3 compared to $IO_{82}S$.

3.1.3 EDS analysis

Figure 2 shows the EDS spectrum of $IO_{82}S$ and $IO_{65}S$. L–α line at 2.983 keV, comes from the Ag atoms present in the nanocomposite, and two K-α lines at 0.525 keV and 6.398 keV, come from the O and Fe atoms respectively [3, 21]. From 2(c), it can be clearly seen that both the composite contain major percentage of Ag, and the amount of Fe_2O_3 is slightly higher in $IO_{82}S$.

3.1.4 Thermogravimetric analysis

The TGA thermograms of the Fe_2O_3 and Ag/Fe_2O_3 nanocomposites are shown in Fig. 1d. The initial weight loss observed below 400 °C corresponds to the loss of superficial and chemisorbed water molecules on the nanoparticles surface. The weight loss between 400 and 800 °C can be attributed to phase transformation from mixed phases of iron oxides into α- Fe_2O_3 phase [22, 23]. Since monophasic β-Fe_2O_3 crystals are difficult to obtain, it is difficult to determine the transformation mechanism to α-Fe_2O_3 [24]. The increase in thermal stability of Fe_2O_3 to $IO_{82}S$ and $IO_{65}S$ might be due to the successful attachment of Fe_2O_3 to the surface Ag. The lesser amount of Fe_2O_3 creates less vacant space for superficial water and less probability of Fe_2O_3 phase transition. This might make $IO_{65}S$ more thermally stable than $IO_{82}S$. From the TGA thermogram, it is understood that the weight loss of the nanocomposites is very low, and the nanocomposites are thermally very stable.

3.1.5 Morphological characterization

The surface morphology, as well as the size of the Ag/Fe_2O_3 nanocomposite was monitored using the FE-SEM technique (Fig. 3). Images of the synthesized Ag/Fe_2O_3 nanocomposite reveal the presence of uniformly

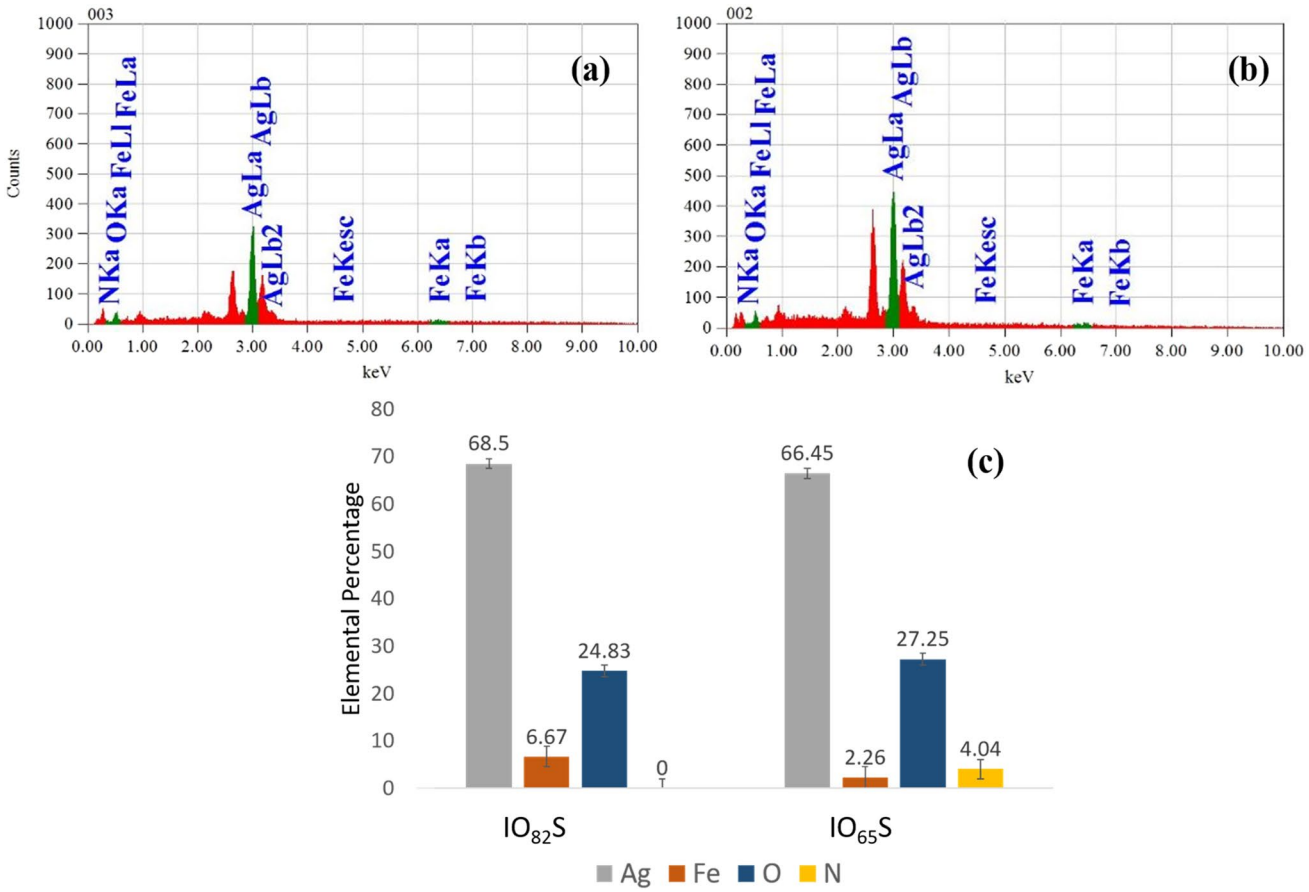

Fig. 2 EDS spectra of **a** $IO_{82}S$, **b** $IO_{65}S$ and **c** elemental composition of the as synthesized $IO_{82}S$ and $IO_{65}S$

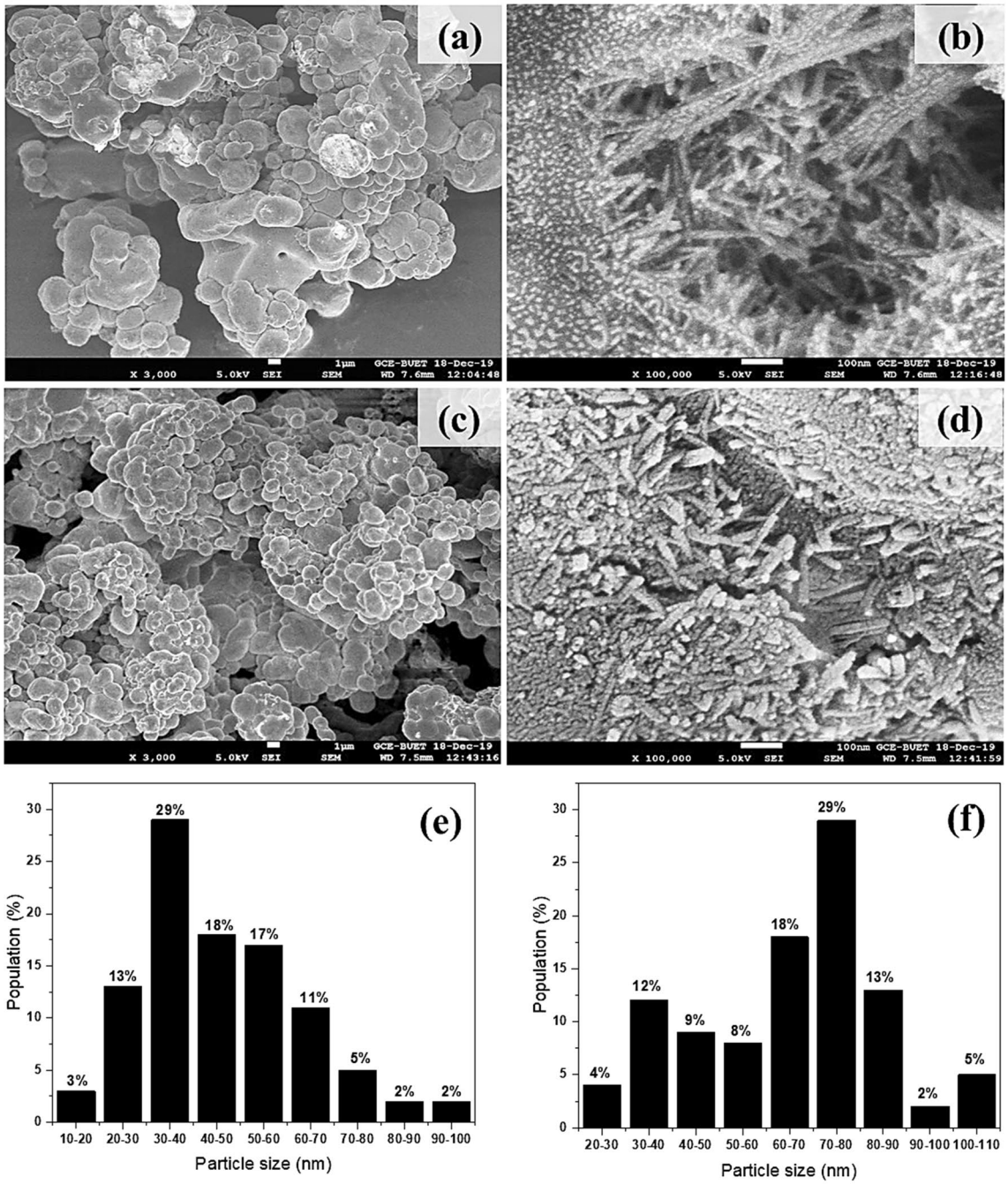

Fig. 3 FE-SEM image of synthesized Ag/Fe_2O_3 nanocomposites; **a**, **b** $IO_{82}S$ at 3000× and 100000× magnifications, **c**, **d** $IO_{65}S$ at 3000× and 100000× magnifications, and **e**, **f** size distribution of $IO_{82}S$ and $IO_{65}S$

distributed nearly spherical-shaped particles. Fe_2O_3 nanospikes are evenly distributed on the surface of Ag microspheres. Large particles can be seen in some of the images; these are most likely the result of smaller particles agglomerating into larger ones due to large surface area and high surface energy [25]. The surface morphology of the Ag/Fe_2O_3 nanocomposites was observed at 3000× and 100000× magnifications. To understand the size of nanoparticles, 100 particles were arbitrarily selected from the image, and their diameter was measured with respect to the scale 100 nm [26].

The particle size of Fe_2O_3 in the Ag/Fe_2O_3 nanocomposites was in the range of 10 to 110 nm. A maximum population of the nanoparticles was seen in the range of 70 to 80 nm for $IO_{82}S$ and 30 to 40 nm for $IO_{65}S$, which is agreeable with the results obtained from XRD analysis. The

smaller size for $IO_{65}S$ than $IO_{82}S$ might be due to the presence of the greater amount of Ag present in the reaction mixture. More Ag in $IO_{65}S$ probably prevented agglomeration by reducing the magnetic interaction of Fe_2O_3 in the surface of Ag [27]. As the composite was treated with conc. HCl after the formation of the nanocomposite, the free oxides leached out from the surface and the incorporated oxides remained at the surface of Ag. ATR-IR spectra, XRD analysis, elemental analysis, along with the FESEM imaging, confirm the successful formation of Ag/Fe_2O_3 nanocomposite where Fe_2O_3 nanospikes are firmly deposited on the Ag microsphere surface.

3.2 Anti-bacterial properties and in vitro biological applications

3.2.1 Anti-bacterial activity of Ag/Fe_2O_3 nanocomposites

The antibacterial properties of the Ag/Fe_2O_3 nanocomposites synthesized were evaluated by measuring the diameter of the inhibition zone using the agar well diffusion techniques (Fig. 4).

Primarily, the zone of inhibition (ZOI) was tested using *E.coli* DH5α to see the anti-bacterial performance. The concentration was gradually increased, and finally, three concentrations (5 mg/mL, 20 mg/mL and 30 mg/mL) were selected to see the ZOI as at low concentration, the ZOI is low (Table 1). The core of the nanocomposite is composed of Ag, and the outer layer consists of mainly Fe_2O_3 nanospikes. Since Ag shows more anti-bacterial efficacy than Fe_2O_3 and it is inside the Fe_2O_3 nanospike layer, the interaction between bacteria and nanocomposite to produce reactive oxygen species (ROS) is relatively low. Due to this, the required concentration of nanocomposite for

Table 1 Diameter zone of inhibition (ZOI) for different bacteria by using $IO_{82}S$ and $IO_{65}S$

Materials	Concentration (mg/mL)	*Klebsiella spp.* (mm)	*E. coli* (mm)	*Pseudomonas* (mm)	*S. aureus* (mm)
Fe_2O_3	5	0	0	0	0
	20	0	0	0	7
	30	7	8	0	9
$IO_{82}S$	5 (KA1)	0	0	0	0
	20 (KA2)	10	7	5	10
	30 (KA3)	12	13	8	11
$IO_{65}S$	5 (KB1)	0	0	0	6
	20 (KB2)	12	9	6	14
	30 (KB3)	15	16	13	19

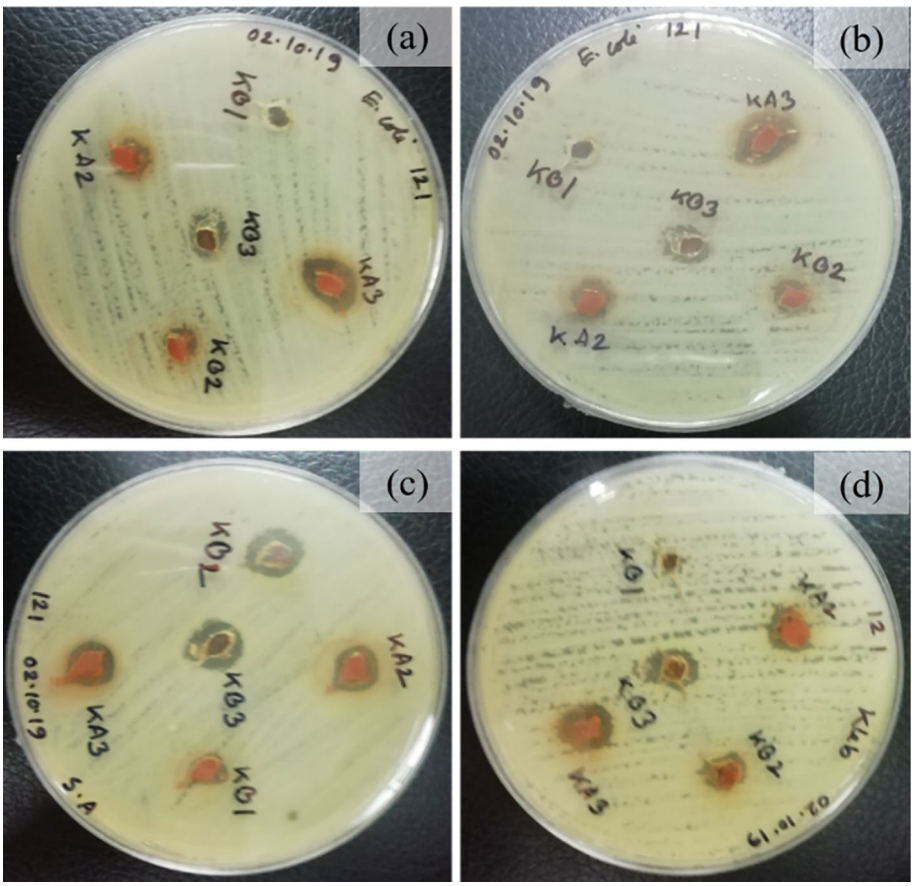

Fig. 4 Anti-bacterial activity of by Ag/Fe_2O_3 nanocomposites against **a**, **b** *E. coli*, **c** *Staphylococcus aureus*, **d** *Klebsiella spp. b*acteria

anti-bacterial assay may be relatively high in this case. With increasing concentration, higher amounts of nanocomposites become firmly deposited on the bacterial membrane, and generation of ROS turns out to be sufficient to show higher anti-bacterial efficacy.

The highest ZOI was found for *Staphylococcus aureus,* which is 19 mm, and the lowest was 8 mm for *the Pseudomonas* with a concentration of 30 mg/mL. This might be due to the difference in the cell wall structure of the two bacteria. Here, *Staphylococcus aureus* is gram-positive, while *Pseudomonas* is a Gram-negative bacterium. The *Pseudomonas* cell wall is made up of lipopolysaccharides, phospholipids, and lipoproteins which together form a barrier that only allows micromolecules to enter the cell. On the contrary, the cell wall of Gram-positive bacteria *Staphylococcus aureus* is made up of a layer of peptidoglycan, teichoic acid, and abundant pores. These pores allow smaller molecules to enter the cell which in turn causes membrane damage and cell death. In addition, Gram-positive bacteria carry a high negative charge on the cell wall surface compared to Gram-negative bacteria, which can attract NPs. This could be a reason for the greater inhibition zone in the case of Gram-positive *Staphylococcus aureus* [28, 29]. The anti-bacterial effect of Fe_2O_3 was also studied in control experiments and it was observed that Fe_2O_3 has lower anti-bacterial activity than the composites. It was observed that the ZOI for $IO_{65}S$ is greater than $IO_{82}S$. From EDS analysis (Fig. 2), it is evident that $IO_{82}S$ contains more amount of Fe_2O_3 than $IO_{65}S$, and as a result more surface area is covered by Fe_2O_3 nano-spikes. Since Ag is known to have more bactericidal properties than Fe_2O_3, this nanospikes on the surface of core Ag slightly inhibit the anti-bacterial activity in case of $IO_{82}S$. From the ZOI, it can be concluded that the produced nanocomposites are effective for both Gram-negative and Gram-positive bacteria and can be an excellent material for anti-bacterial applications. A similar result was found by Kulkarni et al. [30].

3.2.2 *Plausible mechanism of anti-bacterial activity of Ag/Fe_2O_3 nanocomposite*

The bactericidal impact of the Ag/Fe_2O_3 nanocomposite could be attributed to the discharge of Ag from the composite. Since the Ag surface is partly covered with Fe_2O_3 nanospike, the interaction might occur where the Ag surface is exposed. The strong interaction between the silver ion and thiol groups of vital enzymes causes bacteria to lose their replication ability [31]. The abundance of carboxylic and other functional groups results in a negatively charged surface of the cell at physiological pH. The electrostatic forces between the opposite charges of the bacteria and the silver in the nanocomposite might be the reason for its adhesion and anti-bacterial activity [32]. Fe_2O_3 alone can also show significant anti-microbial activity, which is reported by several authors [16]. Fe_2O_3 nanoparticles are very stable in normal environmental conditions but they become active under UV light where the defect sites generate ROS such as superoxide radical anions (O^{2-}) and hydroxyl radicals (OH^-). The ROS can lead to bacterial death by membrane desorption, disruption of cellular function, etc. [33, 34]. Figure 5a depicts the membrane damage and cell death of bacteria due to the activity of nanoparticles.

3.2.3 *Anti-biofilm activity of Ag/Fe_2O_3 nanocomposites*

In the anti-biofilm study, both $IO_{82}S$ and $IO_{65}S$ showed significant efficacy against bacterial biofilm. With increasing concentration, the percent reduction in the biofilm of four different types of bacteria increased (Fig. 6).

A higher log reduction indicates a better anti-biofilm activity of the nanocomposites against bacteria. The highest logarithmic reduction of 0.52 and 0.76 was observed for *Staphylococcus aureus* at a concentration of 30 mg/mL using $IO_{82}S$ and $IO_{65}S$, respectively. In the case of Gram-negative *Klebsiella spp,* it was 0.31 and 0.19 (Table S1–S5). The presence of the nanocomposite killed a biofilm of 82.56% *Staphylococcus aureus* and 51.06% *Klebsiella spp.* The destruction of the biofilm for Gram-positive *Staphylococcus aureus* was greater than that of any other Gram-negative bacteria used in this work. The difference in the structure of the cell wall might be a reason for this destruction. Figure 5b demonstrates the plausible mechanism of anti-biofilm activity of Ag/Fe_2O_3 nanocomposites.

3.2.4 Plausible mechanism of anti-biofilm activity

To protect themselves from adverse environmental conditions such as UV exposure, acid exposure, dehydration, and salinity, different antibiotics and anti-microbial agent microbes in biofilm produce extracellular polymeric substances (EPS) such as proteins, DNA, polysaccharides, RNA, etc. [35]. The breakdown of the biofilm might be due to the interaction of the Ag/Fe_2O_3 nanocomposite with EPS and with the bacterial communication system, quorum sensing (QS), by which bacteria communicate with each other through the production and detection of signal molecules. All bacteria employ this cell-to-cell communication between intra and interspecies bacterial populations to respond to changes in adverse conditions [36]. Targeting and disrupting QS signaling systems is possibly the main mechanism by which Ag/Fe_2O_3 nanocomposite displays anti-biofilm activity. Gram-negative and Gram-positive bacteria have peptidoglycan in their cell walls. Cleavage of these peptidoglycans reduces biofilm formation by

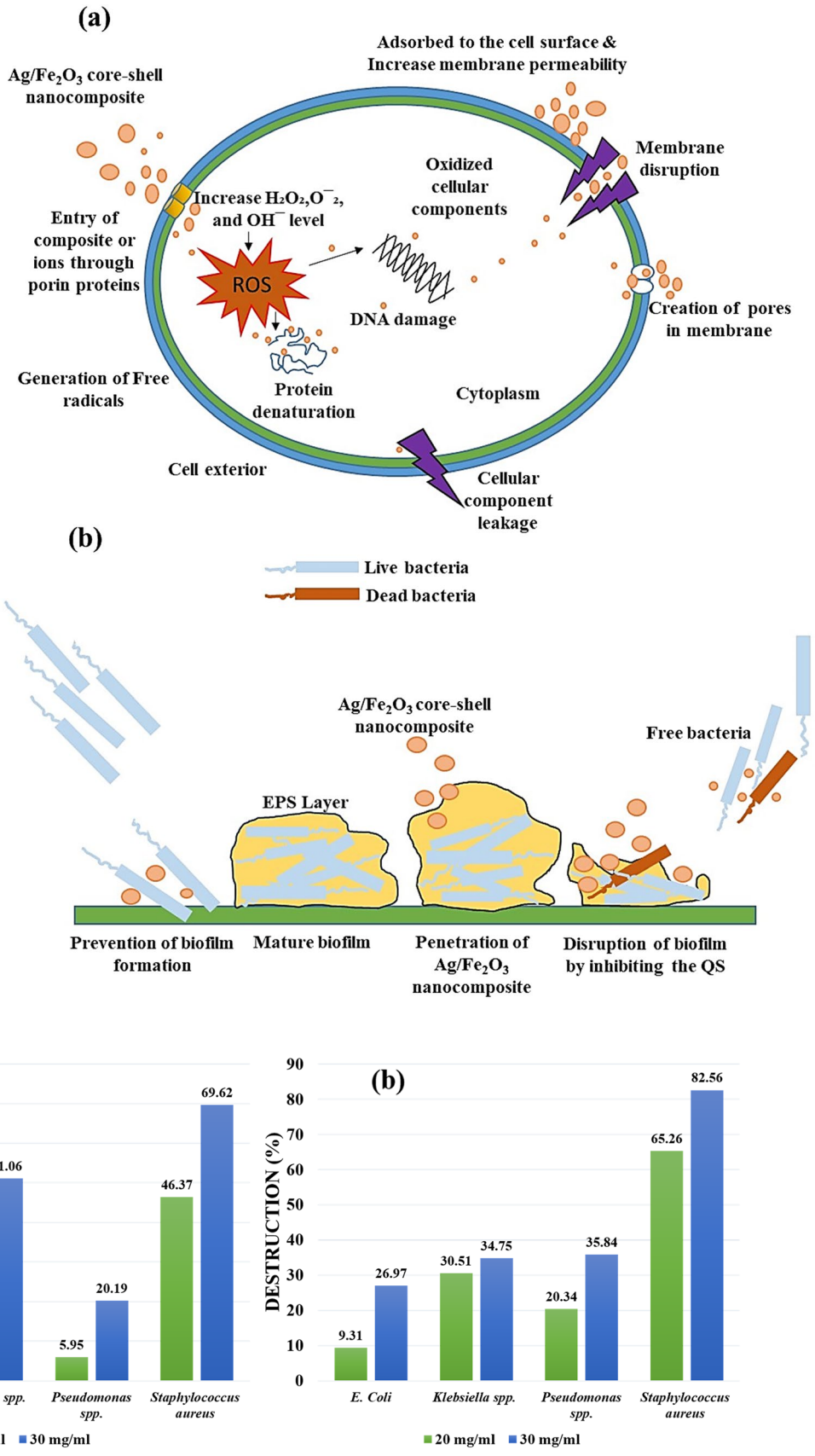

Fig. 5 The anti-bacterial effect of Ag/Fe_2O_3 nanocomposite was studied through in vitro biological applications; **a** bacteria membrane damage and cell death by ROS activity; **b** mechanism of anti-biofilm activity of Ag/Fe_2O_3 nanocomposites. QS stands for quorum sensing

Fig. 6 Efficacy of **a** $IO_{82}S$ and **b** $IO_{65}S$ against biofilm at different concentration

altering the composition of teichoic acids and proteins present in the cell wall, signaling molecules that can modulate the biofilm-related gene expression [5].

3.3 *Cytotoxicity of Ag/Fe_2O_3 nanocomposites*

The cytotoxic effect of the Ag/Fe_2O_3 nanocomposites in their natural state was investigated using three different cell lines: Vero, BHK-21, and Hela. To investigate the cytotoxic effect, the highest concentration used to investigate the antibacterial effect (30 mg/L) was selected. A control experiment was also performed to find out the effect of phosphate buffered saline-PBS (pH ~ 7.4). After washing the cells with PBS, more than 95% of cells of all cell lines were survived, indicating no significant effect of the buffer. Figure 7a–c show the microscope image for the analysis of cytotoxicity on Hela cancer cell lines with the nanocomposites produced. A similar percentage of cell survival was observed for both $IO_{82}S$ and $IO_{65}S$. The prepared $IO_{82}S$ and $IO_{65}S$ show very high toxicity (cell survival 10–20%) against Hela cells. This result indicates that the synthesized nanocomposite may be a potential anti-cancer material [37, 38].

The previous studies reported the potential anti-cancer activity of Ag/Fe_2O_3 nanocomposite [30]. The toxic effect of $IO_{82}S$ and $IO_{65}S$ on BHK-21 is shown in Fig. 7d–f. The survival percentage of BHK cells indicates that the nanocomposites kill nearly 80–90% of cells. BHK cells are capable of both reproducing themselves in hamster tissues and producing tumors when injected into adult hamsters [39, 40]. As BHK cells cause tumors, the nanocomposite can be used as material to destroy these cells, and further research might develop its activity. The cytotoxic effect of Fe_2O_3 was also investigated. The moderate cytotoxic effects were measured with Hela and BHK cell lines (cell survival 30–40%). The toxicity in Vero cells is shown in Fig. 7g–i. Approximately 70–80% of Vero cells survived in the experiment, which is an indication of less toxicity of nanocomposites for mammalian cells and bodies [17, 41]. Kulkarni et al. [30] reported a similar kind of result that the produced nanocomposite did not show significant

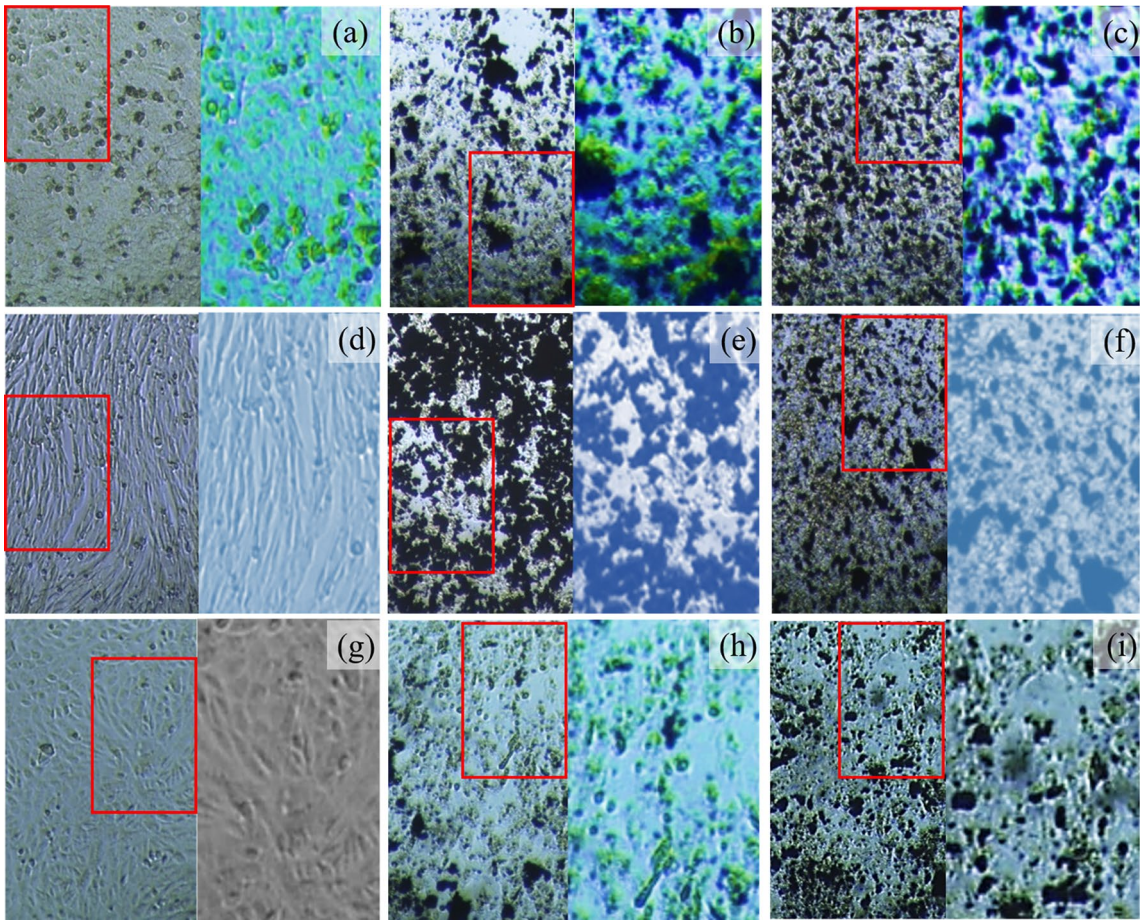

Fig. 7 Inverted light microscope images of cancer cell Hela **a** in the absence of nanocomposite, in the presence of **b** $IO_{82}S$ and **c** $IO_{65}S$; BHK-21 cells **d** in the absence of nanocomposite, in the presence of **e** $IO_{82}S$ and **f** $IO_{65}S$; Vero cells **g** in the absence of nanocomposite, in the presence of **h** $IO_{82}S$ and **i** $IO_{65}S$

cytotoxicity against normal cells. A lower concentration of nanocomposites might kill a lesser percentage of normal cells. The cytotoxic effect of the nanocomposites might be due to the formation of ROS, which damage the essential cell components such as lipids, DNA, and proteins, leading to the death of the cells. Mitochondrial function decrease, lactate dehydrogenase (LDH) release, apoptosis, aberration and DNA damage might also be some reasons [42, 43]. In a study by Saranya et al. [4], the anti-cancer potential of Fe_2O_3/Ag nanocomposite against lung cancer (A549 cell line) was evaluated. The MMT assay revealed that treated cells had reduced cell viability compared to control cells. The findings suggested that concentrations of Fe_2O_3/Ag ranging from 100 to 200 µg/mL were not toxic to A549 cells, but higher concentrations (300–400 µg/mL) exhibited a significant decrease in cell viability. However, pristine Fe_2O_3 at the same concentration showed lower cytotoxicity towards the cells. The authors attributed the higher anticancer efficacy of Fe_2O_3/Ag than Fe_2O_3 to the generation of (ROS) that induce cell death in breast cancer cells (MCF-7).

4 Conclusion

The present work highlights the in situ ROS-mediated antibacterial and anti-cancer activity of Ag/ Fe_2O_3 nanocomposite which was successfully synthesized using a simple, faster, more efficient, and environmentally friendly thermal decomposition route. The morphology along with the ATR-IR, XRD, and EDS data, confirmed a successful formation of Ag/Fe_2O_3 nanocomposite where Fe_2O_3 nanospikes were found to be distributed on the surface of the Ag microsphere. The Ag/Fe_2O_3 nanocomposite presents a significant opportunity for the development of materials that have the potential for efficient application in biomedical fields such as nanomedicine and pharmacotherapy. The high ZOI in case of anti-bacterial study and a higher percentage of biofilm reduction ability makes them a suitable candidate for future exploration. Careful tuning and surface modification in the particle surface might improve their efficacy. Cytotoxicity towards Hela and BHK cell line indicate their potential to be a candidate in cancer research if biocompatibility can be achieved more by modification in the preparation process of the nanocomposites. Finally, this work contributes to the fundamental understanding of bioactive nanomaterial production using a greener approach which could find relevant biomedical applications.

Acknowledgements The authors express gratitude to the Centre for Advanced Research in Sciences (CARS), University of Dhaka, Bangladesh for partial analytical support. The authors thank the International Association of Advanced Materials (IAAM), Sweden for providing a collaboration platform under its R&D World Links.

Author contributions MKH: Conception of the work, data collection and analysis, drafting the article with assistance from all the coauthors, AM: Writing—review & editing, AT and AT: Data analysis, Writing—review & editing, BP: Writing—review & editing, SCD: Writing—review & editing, OS: Data collection & analysis, MMR: Review & editing, YRS: Review & editing, AT: Writing—review & editing, MA: Conception of the work, writing—review & editing.

Funding The authors are thankful to the Ministry of Science and Technology, Government of the People's Republic of Bangladesh, for providing financial support to carry out this research.

Declarations

Competing interests On behalf of all authors, the corresponding author states that there is no conflict of interest.

References

1. Chaudhuri RG, Paria S (2011) Core/shell nanoparticles: classes, properties, synthesis mechanisms, characterization, and applications. Chem Rev 112(4):2373–2433
2. Sangaiya P, Jayaprakash R (2018) A review on iron oxide nanoparticles and their biomedical applications. J Supercond Novel Magn 31(11):3397–3413
3. Demarchi CA, Cruz AB, Ślawska-Waniewska A, Nedelko N, Dłużewski P, Kaleta A, Trzciński J, Dal Magro J, Scapinello J, Rodrigues CA (2018) Synthesis of Ag@ Fe2O3 nanocomposite based on O-carboxymethylchitosan with antimicrobial activity. Int J Biol Macromol 107:42–51
4. Saranya A, Thamer A, Ramar K, Priyadharsan A, Raj V, Murugan K, Murad A, Maheshwaran P (2020) Facile one pot microwave-assisted green synthesis of Fe_2O_3/Ag nanocomposites by phytoreduction: potential application as sunlight-driven photocatalyst, antibacterial and anticancer agent. J Photochem Photobiol B 207:111885
5. Khan AU, Ur Rahman A, Yuan Q, Ahmad A, Khan ZUH, Mahnashi MH, Alyami BA, Alqahtani YS, Ullah S, Wirman AP (2020) Facile and eco-benign fabrication of Ag/ Fe_2O_3 nanocomposite using Algaia Monozyga leaves extract and its' efficient biocidal and photocatalytic applications. Photodiagn Photodyn Ther 32:101970
6. Thi TV, Tam LT, Phan VN, Van Quy N, Huy TQ, Le AT (2017) Two-step hydrothermal synthesis of bifunctional hematite–silver

heterodimer nanoparticles for potential antibacterial and anticancer applications. J Electron Mater 46(6):3323–3332
7. Al-Zahrani FAM, Salem SS, Al-Ghamdi HA, Nhari LM, Lin L, El-Shishtawy RM (2022) Green synthesis and antibacterial activity of Ag/Fe2O3 nanocomposite using Buddleja lindleyana extract. Bioengineering 9(9):452
8. Odularu AT (2018) Metal nanoparticles: thermal decomposition, biomedicinal applications to cancer treatment, and future perspectives. Bioinorg Chem Appl. https://doi.org/10.1155/2018/9354708
9. Ashaduzzaman Md, Deshpande SR, Arul Murugan N, Mishra YK, Turner APF, Tiwari A (2017) On/off-switchable LSPR nanoimmunoassay for troponin-T. Sci Rep 7(1):1–10
10. Shakhawat BM, Hossen MY, Miah SC, Paul TD, Aka OS, Rahaman MM, Sharif MJI, Habiba O, Ashaduzzaman Md (2020) Green synthesis of iron oxide nanoparticle using Carica papaya leaf extract: application for photocatalytic degradation of remazol yellow RR dye and antibacterial activity. Heliyon 6(8):4603
11. Bauer AW (1966) Antibiotic susceptibility testing by a standardized single disc method. Am J clin pathol 45:149–158
12. Jabir MS, Nayef UM, Jawad KH, Taqi ZJ, Ahmed NR (2018) Porous silicon nanoparticles prepared via an improved method: a developing strategy for a successful antimicrobial agent against *Escherichia coli* and *Staphylococcus aureus*. IOP Conf Ser Mater Sci Eng 454:012077
13. Mohanta YK, Biswas K, Jena SK, Hashem A, AbdAllah EF, Mohanta TK (2020) Anti-biofilm and antibacterial activities of silver nanoparticles synthesized by the reducing activity of phytoconstituents present in the Indian medicinal plants. Front Microbiol. https://doi.org/10.3389/fmicb.2020.01143
14. Kostaki M, Chorianopoulos N, Braxou E, Nychas G-J, Giaouris E (2012) Differential biofilm formation and chemical disinfection resistance of sessile cells of Listeria monocytogenes strains under monospecies and dual-species (with Salmonella enterica) conditions. Appl Environ Microbiol 78:2586–2595
15. Hamilton M (2010) The log reduction (LR) measure of disinfectant efficacy. MSU Center for Biofilm Engineering, Montana
16. Giri J, Thakurta SG, Bellare J, Nigam AK, Bahadur D (2005) Preparation and characterization of phospholipid stabilized uniform sized magnetite nanoparticles. J Magn Magn Mater 293:62–68
17. Sharma A, Pawar C, Prasad N, Yewale M, Kamble D (2018) Antimicrobial efficacy of green synthesized iron oxide nanoparticles. Mater Res Express 5:075402
18. Xie T, Xu L, Liu C (2013) Dielectric and magnetic response of Sr–Zn ferrite composite. RSC Adv 3:15856–15865
19. Alaizeri ZM, Alhadlaq HA, Aldawood S, Akhtar MJ, Amer MS, Ahamed M (2021) Facile synthesis, characterization, photocatalytic activity, and cytotoxicity of ag-doped mgo nanoparticles. Nanomaterials 11(11):2915
20. Rashid TM, Nayef UM, Jabir MS, Mutlak FAH (2021) Synthesis and characterization of Au: ZnO (core: shell) nanoparticles via laser ablation. Optik 244:167569
21. Kumar M, Devi P, Shivling V, Kumar B, Kumar A (2019) Impact on optical, electrical and antibacterial response of microwave irradiated silver nanoparticles. J Mater Sci Mater Electron 30:6370–6377
22. Rufus A, Sreeju N, Philip D (2016) Synthesis of biogenic hematite (α-Fe 2 O 3) nanoparticles for antibacterial and nanofluid applications. RSC Adv 6:94206–94217
23. Kido O, Higashino Y, Kamitsuji K, Kurumada M, Sato T, Kimura Y, Suzuki H, Saito Y, Kaito C (2004) Phase transition temperature of γ-Fe2O3 ultrafine particle. J Phys Soc Jpn 73:2014–2016
24. Danno T, Nakatsuka D, Kusano Y, Asaoka H, Nakanishi M, Fujii T, Ikeda Y, Takada J (2013) Crystal structure of β-Fe2O3 and topotactic phase transformation to α-Fe2O3. Cryst Growth Des 13:770–774
25. Abdul Kadhim WK, Nayef UM, Jabir MS (2019) Polyethylene glycol-functionalized magnetic (Fe3O4) nanoparticles: a good method for a successful antibacterial therapeutic agent via damage DNA molecule. Surf Rev Lett 26(10):1950079
26. Abed MA, Mutlak FAH, Ahmed AF, Nayef UM, Abdulridha SK, Jabir MS (2021) Synthesis of Ag/Au (core/shell) nanoparticles by laser ablation in liquid and study of their toxicity on blood human components. J Phys Conf Ser 1795(1):012013
27. Jabir MS, Nayef UM, Abdul KWK (2019) Polyethylene glycol-functionalized magnetic (Fe 3 O 4) nanoparticles: a novel DNA-mediated antibacterial agent. Nano Biomed Eng 11(1):18–27
28. Spagnul C, Greenman J, Wainwright M, Kamil Z, Boyle RW (2016) Synthesis, characterization and biological evaluation of a new photoactive hydrogel against gram-positive and gram-negative bacteria. J Mater Chem B 4(8):1499–1509
29. Sarwar A, Katas H, Samsudin SN, Zin NM (2015) Regioselective sequential modification of chitosan via azide-alkyne click reaction: synthesis, characterization, and antimicrobial activity of chitosan derivatives and nanoparticles. PLoS ONE 10(4):e0123084
30. Kulkarni S, Jadhav M, Raikar P, Barretto DA, Vootla SK, Raikar U (2017) Green synthesized multifunctional Ag@ Fe2O3 nanocomposites for effective antibacterial, antifungal and anticancer properties. New J Chem 41:9513–9520
31. Feng QL, Wu J, Chen GQ, Cui F, Kim T, Kim J (2000) A mechanistic study of the antibacterial effect of silver ions on Escherichia coli and Staphylococcus aureus. J Biomed Mater Res 52:662–668
32. Kareem ZH, Shareef HK, Alkaim AF (2018) Evaluation of antibacterial activity of Fe^ sub 2^ O^ sub 3^ nanoparticles against Shigella dysenteriae. J Pharm Sci Res 10:1980–1982
33. Pallela PNVK, Ummey S, Ruddaraju LK, Gadi S, Cherukuri CS, Barla S, Pammi S (2019) Antibacterial efficacy of green synthesized α-Fe2O3 nanoparticles using Sida cordifolia plant extract. Heliyon 5:e02765
34. Rana P, Sharma S, Sharma R, Banerjee K (2019) Apple pectin supported superparamagnetic (γ-Fe2O3) maghemite nanoparticles with antimicrobial potency. Mater Sci Energy Technol 2:15–21
35. Roy R, Tiwari M, Donelli G, Tiwari V (2018) Strategies for combating bacterial biofilms: a focus on anti-biofilm agents and their mechanisms of action. Virulence 9(1):522–554
36. Muhammad MH, Idris AL, Fan X, Guo Y, Yu Y, Jin X, Qiu J, Guan X, Huang T (2020) Beyond risk: bacterial biofilms and their regulating approaches. Front Microbiol 11:928
37. Yeggoni DP, Rachamallu A, Dubey S, Mitra A, Subramanyam R (2018) Probing the interaction mechanism of menthol with blood plasma proteins and its cytotoxicity activities. J Biomol Struct Dyn 36(2):465–474
38. Ali Z, Jabir M, Al-Shammari A (2019) Gold nanoparticles inhibiting proliferation of human breast cancer cell line. Res J Biotechnol 14:79–82
39. Mayo J, Lombardo J, Klein-Szanto A, Conti C, Moreira J (1973) An oncogenic virus carried by hamster kidney cells. Can Res 33:2273–2277
40. Gotlieb-Stematsky T, Shilo R (1964) Studies on the tumorigenic properties of baby hamster kidney cell lines and a method of selection of high and low tumorigenic clones. Virology 22:314–320
41. Alaizeri ZM, Alhadlaq HA, Aldawood S, Akhtar MJ, Ahamed M (2023) Photodeposition mediated synthesis of silver-doped indium oxide nanoparticles for improved photocatalytic and anticancer performance. Environ Sci Pollut Res 30(3):6055–6067
42. Botha TL, Elemike EE, Horn S, Onwudiwe DC, Giesy JP, Wepener V (2019) Cytotoxicity of Ag, Au and Ag-Au bimetallic nanoparticles prepared using golden rod (Solidago canadensis) plant extract. Sci Rep 9:1–8

43. Ibrahim AA, Kareem MM, Al-Noor TH, Al-Muhimeed T, AlObaid AA, Albukhaty S, Sulaiman GM, Jabir M, Taqi ZJ, Sahib UI (2021) Pt (II)-thiocarbohydrazone complex as cytotoxic agent and apoptosis inducer in Caov-3 and HT-29 Cells through the P53 and caspase-8 pathways. Pharmaceuticals 14(6):509